1

Effect of Photolysis on Zirconium Amino Phenoxides for the Hydrophosphination of Alkenes: Improving Catalysis

2

3

Bryan T. Novas [1], Jacob A. Morris [1], Matthew D. Liptak [1] and Rory Waterman [1,*]

4

[1] Department of Chemistry, University of Vermont, 82 University Place, Burlington, VT 05401, USA; Bryan.Novas@uvm.edu (B.T.N.); Jacob.Morris@uvm.edu (J.A.M.); Matthew.Liptak@uvm.edu (M.D.L)
* Correspondence: Rory.Waterman@uvm.edu

5

6

7

Abstract: A comparative study of amino phenoxide zirconium catalysts in the hydrophosphination of alkenes with diphenylphosphine reveals enhanced activity upon irradiation. The origin of improved reactivity is hypothesized to result from substrate insertion upon an n → d charge transfer of a Zr–P bond in the excited state of putative phosphido (Zr–PR$_2$) intermediates. TD-DFT analysis reveals the lowest lying excited state in the proposed active catalysts are dominated by a P $3p$ → Zr $4d$ MLCT, presumably leading to enhanced catalysis. This hypothesis follows from triamidoamine-supported zirconium catalysts but demonstrates the generality of photocatalytic hydrophosphination with d^0 metals.

8

9

10

11

12

13

14

15

16

17

1. Introduction

18

Organophosphines have found extensive use in the areas of materials science, biology, agriculture, electronics, and especially, catalysis [1-7]. Despite their utility, responsible use of phosphorus is imperative as a result of dwindling supply [2,3,8]. Selective carbon–phosphorus bond formation has been an on-going focus of research for these reasons [4,9-14]. A wide range of phosphine chemistry has been developed, with metal catalyzed hydrophosphination being one of the most economic avenues for P–C bond formation. Though significant progress has occurred [1,7,15-24], challenges remain for this transformation, with catalyst and substrate scope being two key avenues for improvement [1,15,25-30].

19

20

21

22

23

24

25

26

27

Photolysis has been demonstrated to increase the activity of triamidoamine zirconium compounds for hydrophosphination catalysis while also unlocking reactivity with previously inert substrates [31-33]. This methodology has been extended to other group 15 substrates, leading to improved hydroarsination catalysis with primary arsines [34]. Photolysis plays a key role in these reactions, where reactions are sluggish if not inactive under the strict exclusion of light [27,31,32,34-36]. Analysis by time-dependent density functional theory (TD-DFT) suggests the enhanced reactivity under photolysis is due to the population of a charge-transfer state that exhibits significant σ* character and

28

29

30

31

32

33

34

35

weakening of the Zr–P bond that allows more facile substrate insertion [31]. A question arose from the triamidoamine-supported zirconium studies, is this photocatalysis general? The particular geometry and frontier orbital arrangement of triamidoamine zirconium may result in exclusive photocatalytic activity. To test for general photocatalysis, other known hydrophosphination catalysts with different geometries and donor ligands must be screened.

Yao and coworkers reported a library of zirconium complexes bearing amino phenoxide ligands for the hydrophosphination of alkenes and heterocumulenes [37]. These compounds gave modest turnovers of the hydrophosphination of several styrene derivatives with diphenylphosphine under ambient conditions and low catalyst loadings [37], and a similar study was reported with primary phosphine substrates [38]. Their successful zirconium catalysts with pseudo-octahedral geometries and N_xO_y donor ligand sets were ideal to test hypothesis that photocatalytic enhancement is general. Yao and co-workers' most active hydrophosphination catalyst bearing an N_2O (N_2O = O-2,4-$^tBu_2C_6H_2$-6-CH$_2$N(CH$_2$CH$_2$NMe$_2$)CH$_2$-2-MeO-3,5-$^tBu_2C_6H_2$) donor set was chosen along with a less active analog bearing an N_2O_2 (N_2O_2 = 1,4-bis(O-2,4-$^tBu_2$-6-CH$_2$)piperazine) donor set (Figure 1).
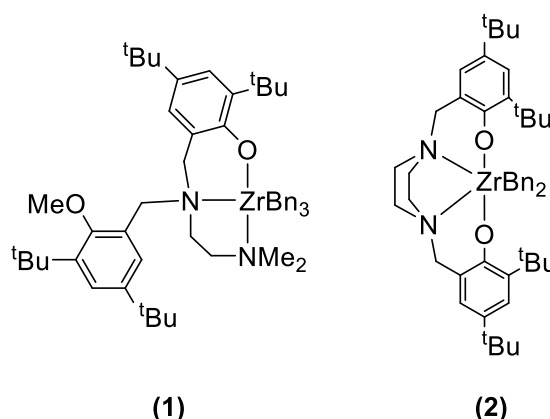

**(1)**   **(2)**

Figure 1. Molecular structure of compounds **1** and **2**.

2. Results and Discussion
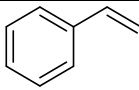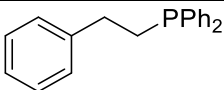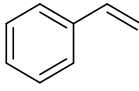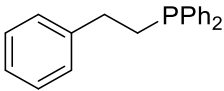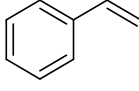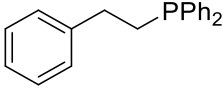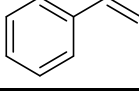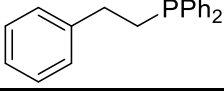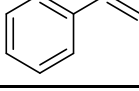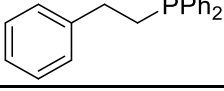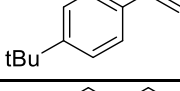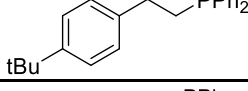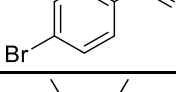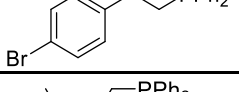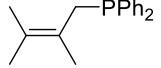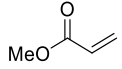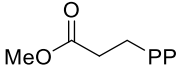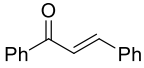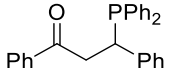
2.1. Photocatalytic Hydrophosphination

Styrene was treated with 1 equiv. of Ph$_2$PH and 5 mol % of (N$_2$O)ZrBn$_3$ (**1**) at ambient temperature under visible light irradiation to afford 83% conversion to the corresponding hydrophosphination product in 2 h (Table 1, Entry 1). Performing the same reaction under ambient light provided 8% conversion after 2 h (Table 1, Entry 2) and 87% conversion after a period of 24 h (Table 1, Entry 4). Reactions run in the dark showed severely reduced product formation, with scarcely observable (~1%) product phosphine formed in 2 h (Table 1, Entry 3) and only 4% conversion after 24 h (Table 1, Entry 5). Catalysis was also expanded to *para-* substituted styrenes. Reaction of 4-*tert*-butyl styrene with Ph$_2$PH under identical conditions led to 70% conversion of the product phosphine (Table 1, Entry 6). Treatment of 4-bromo styrene with Ph$_2$PH under identical conditions gave 91%

conversion in 2 h (Table 1, Entry 7). Similar reactions were successful with non-styrene substrates. Hydrophosphination with 2,3-dimethyl butadiene resulted in 65% conversion in 2 h (Table 1, Entry 8). Methyl acrylate, a commonly active hydrophosphination substrate, gave 90% conversion to the hydrophosphination product under identical conditions (Table 1, Entry 9). *Trans*-chalcone, a typical model substrate in asymmetric hydrophosphination [29,30], showed 68% conversion in a modest 24 h period (Table 1, Entry 10).

Table 1. Intermolecular hydrophosphination of alkenes and Ph_2PH catalyzed by **1**.

$$R\diagup\diagdown + Ph_2PH \xrightarrow[\text{Light Source, } C_6D_6]{\text{5 mol \% }\mathbf{1}} R\diagup\diagdown PPh_2$$
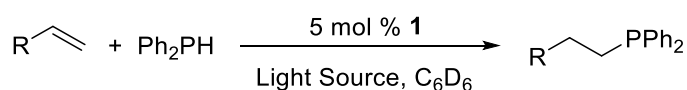
Entry	Substrate	Product	Light Source	Time	Conversion
1			LED	2 h	83%
2			Ambient	2 h	8%
3			Dark	2 h	>1%
4			Ambient	24 h	87%
5			Dark	24 h	4%
6			LED	2 h	70%
7			LED	2 h	91%
8			LED	2 h	65%
9			LED	2 h	90%
10			LED	24 h	68%

Greater conversions were observed, even at lower catalyst loadings, for all styrene substrates through photolysis, complementing the progress made by Yao and co-workers in identifying this compound for hydrophosphination catalysis [37]. It is clear from these results that photolysis can serve to improve hydrophosphination catalysis for **1** using secondary phosphines.

Yao and co-workers demonstrated activity with primary phosphines as well [38]. In that report, neither **1** or **2** were used, but the reported catalysts resemble those investigated in the study and their prior work. Given the enhanced activity of **1** and **2** under photocatalytic conditions, expanding to primary phosphines was explored. Reaction of styrene with $PhPH_2$ and 5 mol % of **1** resulted in quantitative consumption of styrene at 2 h of irradiation (Table 2, Entry 1). The same reaction under ambient light resulted in 21% conversion (Table 2, Entry 2). Extending the reaction period to 24 h resulted in 69% conversion (Table 2, Entry 4). Performing this reaction in the dark resulted in a severely diminished 2% conversion after 2 h (Table 2, Entry 3) and 4% conversion after 24 h (Table 2, Entry 4). Low conversion under ambient light suggests a reason why **1** was not reported in Yao's 2018 study [38], but it affirms the impact of photolysis on d^0 hydrophosphination catalysts.

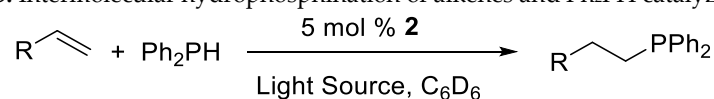**Table 2.** Intermolecular hydrophosphination of styrene and $PhPH_2$ catalyzed by **1**.
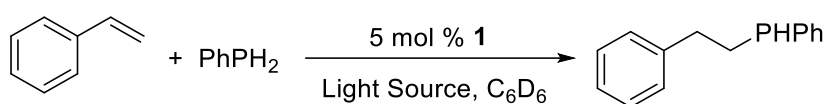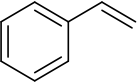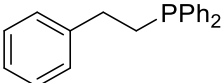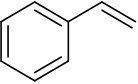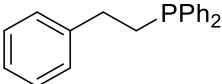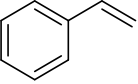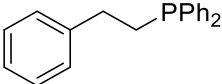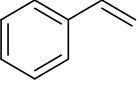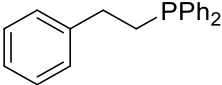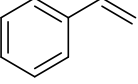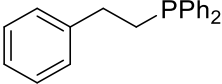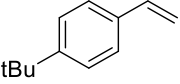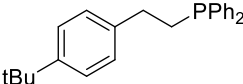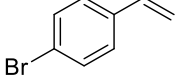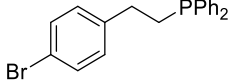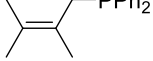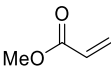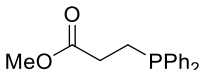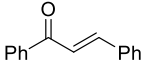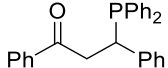

Entry	Product	Light Source	Time	Conversion
1	PHPh	LED	2 h	>99%
2	PHPh	Ambient	2 h	21%
3	PHPh	Dark	2 h	2%
4	PHPh	Ambient	24 h	69%
5	PHPh	Dark	24 h	4%

The change in geometry and lower relative reactivity of (N$_2$O$_2$)ZrBn$_2$ (**2**) as compared to **1** prompted exploration under photocatalytic conditions. Reaction of styrene with Ph$_2$PH and 5 mol % of **2** resulted in 91% product formation after 2 h (Table 3, Entry 1). Conversion under ambient light was behind, providing 12% conversion after 2 h (Table 3, Entry 2), and 92% conversion after an extended 24 h (Table 3, Entry 4). As expected, reactions run rigorously in the dark afforded barely detectable conversion after 2 h (Table 3, Entry 3), and ~ 1% conversion after 24 h (Table 3, Entry 5). Substituted styrenes showed a similar trend to **1**. However, slightly greater conversions were observed under photolysis as compared to ambient light. A conversion of 88% was observed for reaction of 4-*tert*-butyl styrene (Table 3, Entry 6), and quantitative conversion was observed for reaction of 4-bromo styrene after 2 h (Table 3, Entry 4). Under the same conditions with 2,3-dimethyl butadiene as substrate, 66% conversion was observed. (Table 3, Entry 6). Quantitative conversion was seen when using methyl acrylate as substrate (Table 3, Entry 7), and 83% conversion was observed with pro-chiral *trans*-chalcone over a period of 24 h (Table 3, Entry 8).

Table 3. Intermolecular hydrophosphination of alkenes and Ph$_2$PH catalyzed by **2**.
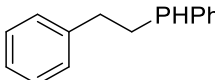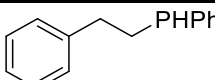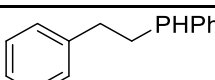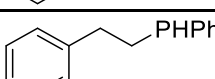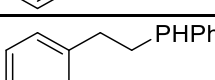
$$R\diagdown\diagup\diagup + \ Ph_2PH \ \xrightarrow[\text{Light Source, C}_6D_6]{\text{5 mol \% } \mathbf{2}} \ R\diagdown\diagup\diagdown PPh_2$$

Entry	Substrate	Product	Light Source	Time	Conversion
1		PPh$_2$	LED	2 h	91%
2		PPh$_2$	Ambient	2 h	12%
3		PPh$_2$	Dark	2 h	>1%
4		PPh$_2$	Ambient	24 h	92%
5		PPh$_2$	Dark	24 h	1%
6	tBu	PPh$_2$ tBu	LED	2 h	88%
7	Br	PPh$_2$ Br	LED	2 h	>99%
8		PPh$_2$	LED	2 h	66%

| 9 | | | LED | 2 h | >99% |
| 10 | | | LED | 24 h | 83% |

As with **1**, the reactivity of **2** in hydrophosphination with $PhPH_2$ was explored. Reaction of styrene with $PhPH_2$ and 5 mol % of **2** resulted in quantitative conversion of styrene to product (Table 4, Entry 1). Using these conditions under ambient light availed 17% conversion in 2 h (Table 4, Entry 2) and 76% conversion in 24 h (Table 4, Entry 4). Running this reaction in the absence of light reduced the conversion to ~2% after 24 h (Table 4, Entry 5).

Table 4. Intermolecular hydrophosphination of styrene and $PhPH_2$ catalyzed by **2**.
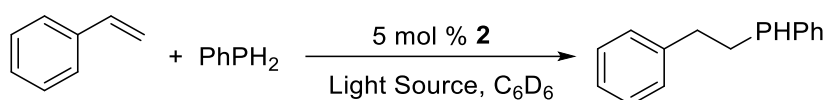
Entry	Product	Light Source	Time	Conversion
1		LED	2 h	>99%
2		Ambient	2 h	17%
3		Dark	2 h	>1%
4		Ambient	24 h	76%
5		Dark	24 h	2%

131
132
133
134
135
136
137
138

139
140

141
142
143
144
145
146
147
148
149
150
151

2.2 Computational Analysis 154

Spectroscopic and computational analysis has indicated an n → d charge transfer in 155
hydrophosphination catalysis using triamidoamine-supported zirconium which leads to 156
improved reactivity as a result of promoted insertion [31]. It was previously hypothesized 157
that pre-existing catalysts could be enhanced by photolysis, and this has been confirmed 158
by experimental results using **1** and **2**. To further elucidate whether enhanced catalysis is 159
a result of accessing an excited state in potential intermediates where insertion is pro- 160
moted, TD-DFT modeling was utilized. 161

All efforts to produce phosphido complexes of **1** and **2** failed, leading to the employ- 162
ment of the crystal structure of **2** to construct a structural model [39]. The geometry of the 163
structural model was optimized using density functional theory (DFT) with the B3LYP 164
functional and the def2-TZVP basis set. The modeling employed the RIJCOSX approxi- 165
mation and tight SCF convergence criteria. The conductor-like polarizable continuum 166
model (CPCM) was used to define a solvent through its dielectric constant and refractive 167
index. The root-mean-square deviation (RMSD) of the optimized geometry of **2** compared 168
to the crystal structure was 0.813 Å. Visually, the DFT-optimized geometry has more ex- 169
posed benzyl groups (Figure 2). 170

171
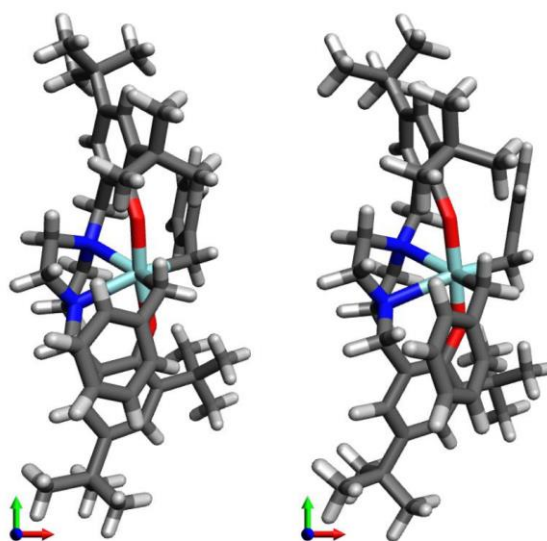
Figure 2. The crystal structure (left) and DFT-optimized geometry (right) of **2**. 172

The electronic structure of **2** was probed via TD-DFT. The first ten electronic transi- 173
tions were calculated with an expansion space of 60 vectors using the B3LYP functional 174
and def2-TZVP basis set, again employing the RIJCOSX approximation and tight SCF con- 175
vergence criteria. Solvent was simulated with the CPCM solvation model. The orca_map- 176
spc was used to convolute the transitions through Gaussians with a full-width half-max 177
(FWHM) of 1500 cm^{-1}. This was compared with an experimental absorption spectrum of 178
2 in diethyl ether, revealing a low-energy, low-intensity shoulder and a higher-energy, 179
higher-intensity peak around 30,000 cm^{-1} in both the experimental and predicted spectra 180
(Figure 3). The predicted spectrum is slightly redshifted compared to the experimental 181

spectrum; a common phenomenon that was also observed in the modeling of triamidoamine zirconium [31].
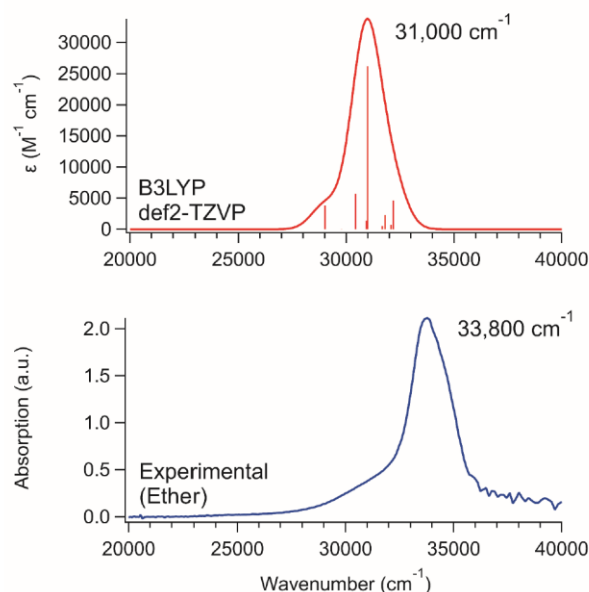
Figure 3. TD-DFT-predicted absorbance spectrum at the B3LYP/def2-TZVP level of theory in the gas phase for **2** (red spectrum) and experimental absorbance spectrum for **2** in diethyl ether (blue spectrum).

It is important to consider that from the absorbance spectra, B3LYP/def2-TZVP predicts a consistent electronic structure for **2** assuming the zirconium oxidation state and molecule charge doesn't change when forming the active catalyst (**2**(PPh$_2$)$_n$). If this is the case, the computational model will still be accurate. However, we can't conclusively prove this without experimental spectra of the active catalyst.

Structural models of the active catalysts (hereafter **A**, **B**, and **AB**) were prepared from the B3LYP-optimized geometry of **2** using the program Avogadro. Either one (**A**), the other (**B**), or both (**AB**) benzyl substituents were replaced with PPh$_2$ substituents. The geometry of **A**, **B**, and **AB** were optimized using DFT at the B3LYP/def2-TZVP level of theory, employing the RIJCOX approximation, tight SCF convergence criteria, and simulating benzene solvent using CPCM (Figure 4).

199
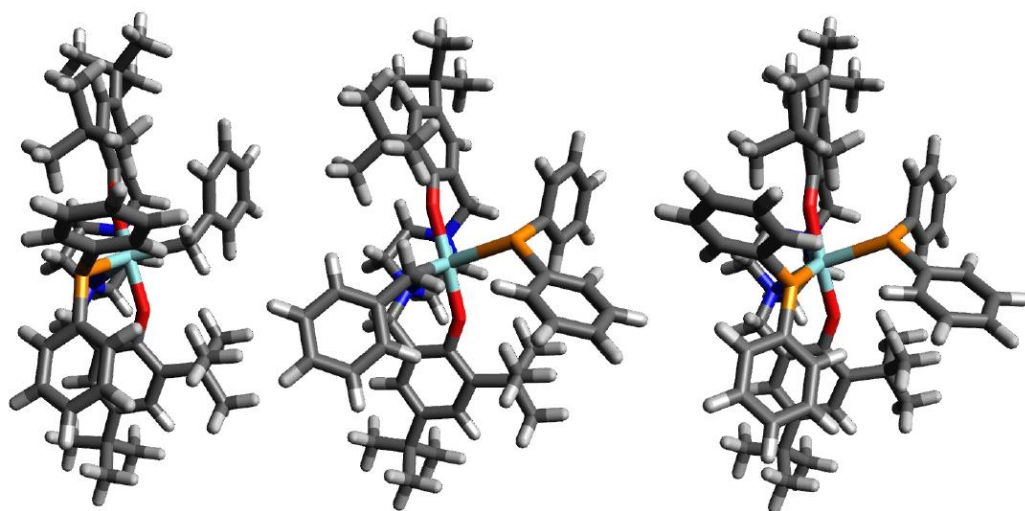
Figure 4. DFT optimized geometry of **A** (left), **B** (middle), and **AB** (right) at the
B3LYP/def2-TZVP level of theory.

200
201

Geometry optimizations give a final Single Point Energy (SPE). The SPE is related to
the number of atoms, and so only **A** and **B**, which have the same number of atoms, can be
compared. There is no energetic preference for replacing Bn **A** or **B** with PPh2 over the
other.

202
203
204
205

TD-DFT calculations at the B3LYP/def2-TZVP level of theory, with the RIJCOSX ap-
proximation, tight SCF convergence criteria, and simulating benzene with CPCM were
carried out to probe the electronic transitions of compounds **A**, **B**, and **AB**. Without ex-
perimental spectra, it cannot be conclusively stated that the computational electronic
structure is consistent, but there is good reason to believe it would be. Regardless, the
predicted absorbance spectra were mapped using orca_mapspc to convolute Gaussians
with a FWHM of 1500 cm^{-1} (Figure in SI). The first 10 electronic transitions were calculated
with an expansion space of 60 vectors.

206
207
208
209
210
211
212
213

It was hypothesized that excitation into a high-lying excited states is followed by
relaxation to the lowest-lying excited state, following Kasha's Rule, from which catalysis
was proposed to occur [31]. The lowest *three* excited states for compound **A** are dominated
by transitions that exhibit donation from a P *3p* orbital to a Zr *4d* orbital, consistent with
work using triamidoamine zirconium [31]. Excited states for compound **B** are largely the
same, to the extent of having the same orbital numbers. In compound **AB**, the lowest *four*
excited states are primarily P → Zr donation, because of the second PPh2 moiety.

214
215
216
217
218
219
220

The charge and formal oxidation state of zirconium does not change when **2** becomes
A, **B**, or **AB**, and so it can be assumed that the computational model will remain accurate.
In any active catalyst models (**A**, **B**, or **AB**), the lowest lying excited state—where chemis-
try is proposed to occur via Kasha's Rule—is dominated by a charge transfer from the P
3p orbital to the Zr *4d* orbital. This is a P n → Zr d transition. Based on prior results [31],
we can assume that this charge transfer is correlated with elongation of the Zr–P bond in
the lowest-lying excited state, thereby weakening the bond to facilitate insertion chemis-
try. This hypothesis is corroborated by our experimental results in photocatalytic hydro-
phosphination using **1** and **2**.

221
222
223
224
225
226
227
228
229

3. Conclusions

230

Irradiation serves to enhance intermolecular hydrophosphination catalysis with **1** and **2** for both secondary and primary phosphines. An accurate computational model of the electronic structure of **2** was determined. The lowest lying excited state in compounds **A**, **B**, and **AB** were found to be dominated by P n → Zr d transitions, likely promoting insertion chemistry. In sum, these findings establish that photocatalytic hydrophosphination is not restricted to triamidoamine-supported zirconium, five-coordinate zirconium, or nitrogen donors. It is general to other zirconium catalysts equipped with distinct geometries and donor ligand sets, and these results suggest that this enhancement may be broadly applicable to d^0 metals though a similar mechanism.

4. Synthetic, Spectroscopic, and Catalytic Methods

All air-sensitive manipulations were performed according to a previously published literature procedure [31,32]. Diphenylphosphine was synthesized according to a modified literature procedure [40]. **1** and **2** were synthesized according to modified literature procedures [37,39]. All other chemicals were obtained from commercial suppliers and dried by conventional means.

NMR spectra were recorded with a Bruker AXR 500 MHz spectrophotometer in benzene-d_6 solution and reported with reference to residual solvent signal (δ = 7.16 ppm) in ^{1}H NMR spectra. Absorption spectra were recorded with an Agilent Technologies Cary 100 Bio UV-Visible Spectrophotometer (Santa Clara, California, USA) as ether solutions. $(N_2O_2)ZrBn_2$ was excited between 700 and 200 nm and excitation slits were set to 2 nm.

Hydrophosphination of alkenes were carried out in a PTFE-sealed J-Young style NMR tube charged with 0.1 mmol alkene, 0.1 mmol phosphine (1.0 M benzene-d_6 solvent stock solution), and 5 mol % of catalyst (0.04 M benzene-d_6 stock solution). The solutions were reacted at ambient temperature for noted period under irradiation. The consumption of substrate to product were monitored by ^{1}H NMR and ^{31}P{^{1}H} NMR spectroscopy. Reaction run in new NMR tubes showed identical conversions as those run in reused, washed NMR tubes.

References

1.   Bange, C.A.; Waterman, R. Challenges in Catalytic Hydrophosphination. *Chem. Eur. J.* **2016**, *22*, 12598-12605, doi:10.1002/chem.201602749.

2. Slootweg, J.C. Sustainable Phosphorus Chemistry: A Silylphosphide Synthon for the Generation of Value-Added Phosphorus Chemicals. *Angew. Chem. Int. Ed. Engl.* **2018**, *57*, 6386-6388, doi:10.1002/anie.201803692.

3. Falk Øgaard, A.; Brod, E. Efficient Phosphorus Cycling in Food Production: Predicting the Phosphorus Fertilization Effect of Sludge from Chemical Wastewater Treatment. *J. Agric. Food. Chem.* **2016**, *64*, 4821-4829, doi:10.1021/acs.jafc.5b05974.

4. Troev, K.D. Chapter 2 - Reactivity of P–H Group of Phosphines. In *Reactivity of P-H Group of Phosphorus Based Compounds*, Troev, K.D., Ed.; Academic Press: 2018; pp. 19-144.

5. Greenberg, S.; Stephan, D.W. Phosphines bearing alkyne substituents: synthesis and hydrophosphination polymerization. *Inorg. Chem.* **2009**, *48*, 8623-8631, doi:10.1021/ic9012284.

6. Kovacik, I.; Wicht, D.K.; Grewal, N.S.; Glueck, D.S.; Incarvito, C.D.; Guzei, I.A.; Rheingold, A.L. Pt(Me-Duphos)-Catalyzed Asymmetric Hydrophosphination of Activated Olefins: Enantioselective Synthesis of Chiral Phosphines. *Organometallics* **2000**, *19*, 950-953, doi:10.1021/om990882e.

7. Koshti, V.; Gaikwad, S.; Chikkali, S.H. Contemporary avenues in catalytic PH bond addition reaction: A case study of hydrophosphination. *Coord. Chem. Rev.* **2014**, *265*, 52-73, doi:https://doi.org/10.1016/j.ccr.2014.01.006.

8. Bange, C.A. Exploration of Zirconium-Catalyzed Intermolecular Hydrophosphination with Primary Phosphines: Photocatalytic Single and Double Hydrophosphination. *Ph.D. Dissertation Thesis, University of Vermont* **2018**, 1-339.

9. Gladysz, J.A.; Bedford, R.B.; Fujita, M.; Gabbaï, F.P.; Goldberg, K.I.; Holland, P.L.; Kiplinger, J.L.; Krische, M.J.; Louie, J.; Lu, C.C.; et al. Organometallics Roundtable 2013–2014. *Organometallics* **2014**, *33*, 1505-1527, doi:10.1021/om500253z.

10. King, A.K.; Gallagher, K.J.; Mahon, M.F.; Webster, R.L. Markovnikov versus anti-Markovnikov Hydrophosphination: Divergent Reactivity Using an Iron(II) β-Diketiminate Pre-Catalyst. *Chem. Eur. J.* **2017**, *23*, 9039-9043, doi:https://doi.org/10.1002/chem.201702374.

11. Kamitani, M.; Itazaki, M.; Tamiya, C.; Nakazawa, H. Regioselective Double Hydrophosphination of Terminal Arylacetylenes Catalyzed by an Iron Complex. *J. Am. Chem. Soc.* **2012**, *134*, 11932-11935, doi:10.1021/ja304818c.

12. Bange, C.A.; Waterman, R. Zirconium-Catalyzed Intermolecular Double Hydrophosphination of Alkynes with a Primary Phosphine. *ACS Catal.* **2016**, *6*, 6413-6416, doi:10.1021/acscatal.6b01850.

13. Mimeau, D.; Gaumont, A.-C. Regio- and Stereoselective Hydrophosphination Reactions of Alkynes with Phosphine−Boranes: Access to Stereodefined Vinylphosphine Derivatives. *J. Org. Chem.* **2003**, *68*, 7016-7022, doi:10.1021/jo030096q.

14. Basalov, I.V.; Dorcet, V.; Fukin, G.K.; Carpentier, J.-F.; Sarazin, Y.; Trifonov, A.A. Highly Active, Chemo- and Regioselective YbII and SmII Catalysts for the Hydrophosphination of Styrene with Phenylphosphine. *Chem. Eur. J.* **2015**, *21*, 6033-6036, doi:https://doi.org/10.1002/chem.201500380.

15. Rosenberg, L. Mechanisms of Metal-Catalyzed Hydrophosphination of Alkenes and Alkynes. *ACS Catal.* **2013**, *3*, 2845-2855, doi:10.1021/cs400685c.

16. Wang, C.; Huang, K.; Ye, J.; Duan, W.-L. Asymmetric Synthesis of P-Stereogenic Secondary Phosphine-Boranes by an Unsymmetric Bisphosphine Pincer-Nickel Complex. *J. Am. Chem. Soc.* **2021**, *143*, 5685-5690, doi:10.1021/jacs.1c02772.

17. Lapshin, I.V.; Basalov, I.V.; Lyssenko, K.A.; Cherkasov, A.V.; Trifonov, A.A. CaII, YbII and SmII Bis(Amido) Complexes Coordinated by NHC Ligands: Efficient Catalysts for Highly Regio- and Chemoselective Consecutive Hydrophosphinations with PH3. *Chem. Eur. J.* **2019**, *25*, 459-463, doi:https://doi.org/10.1002/chem.201804549.

18. Sadeer, A.; Kojima, T.; Ng, J.S.; Gan, K.; Chew, R.J.; Li, Y.; Pullarkat, S.A. Catalytic access to ferrocenyl phosphines bearing both planar and central chirality – A kinetic resolution approach via catalytic asymmetric P(III)–C bond formation. *Tetrahedron* **2020**, *76*, 131259, doi:https://doi.org/10.1016/j.tet.2020.131259.

19. Isley, N.A.; Linstadt, R.T.H.; Slack, E.D.; Lipshutz, B.H. Copper-catalyzed hydrophosphinations of styrenes in water at room temperature. *Dalton Trans.* **2014**, *43*, 13196-13200, doi:10.1039/C4DT00993B.

20. Li, J.; Lamsfus, C.A.; Song, C.; Liu, J.; Fan, G.; Maron, L.; Cui, C. Samarium-Catalyzed Diastereoselective Double Addition of Phenylphosphine to Imines and Mechanistic Studies by DFT Calculations. *ChemCatChem* **2017**, *9*, 1368-1372, doi:10.1002/cctc.201700003.

21. Moglie, Y.; González-Soria, M.J.; Martín-García, I.; Radivoy, G.; Alonso, F. Catalyst- and solvent-free hydrophosphination and multicomponent hydrothiophosphination of alkenes and alkynes. *Green Chem.* **2016**, *18*, 4896-4907, doi:10.1039/C6GC00903D.

22. Teo, R.H.X.; Chen, H.J.; Li, Y.; Pullarkat, S.A.; Leung, P.-H. Asymmetric Catalytic 1,2-Dihydrophosphination of Secondary 1,2-Diphosphines – Direct Access to Free P*- and P*,C*-Diphosphines. *Adv. Synth. Catal.* **2020**, *362*, 2373-2378, doi:https://doi.org/10.1002/adsc.202000131.

23. Garner, M.E.; Parker, B.F.; Hohloch, S.; Bergman, R.G.; Arnold, J. Thorium Metallacycle Facilitates Catalytic Alkyne Hydrophosphination. *J. Am. Chem. Soc.* **2017**, *139*, 12935-12938, doi:10.1021/jacs.7b08323.

24. Waterman, R. Triamidoamine-Supported Zirconium Compounds in Main Group Bond-Formation Catalysis. *Acc. Chem. Res.* **2019**, *52*, 2361-2369, doi:10.1021/acs.accounts.9b00284.

25. Trifonov, A.A.; Basalov, I.V.; Kissel, A.A. Use of organolanthanides in the catalytic intermolecular hydrophosphination and hydroamination of multiple C–C bonds. *Dalton Trans.* **2016**, *45*, 19172-19193, doi:10.1039/C6DT03913H.

26. Webster, R.L. β-Diketiminate complexes of the first row transition metals: applications in catalysis. *Dalton Trans.* **2017**, *46*, 4483-4498, doi:10.1039/C7DT00319F.

27. Dannenberg, S.G.; Waterman, R. A bench-stable copper photocatalyst for the rapid hydrophosphination of activated and unactivated alkenes. *Chem. Commun. (Camb)* **2020**, *56*, 14219-14222, doi:10.1039/D0CC06570F.

28. Sarazin, Y.; Carpentier, J.-F. Calcium, Strontium and Barium Homogeneous Catalysts for Fine Chemicals Synthesis. *Chem. Rec.* **2016**, *16*, 2482-2505, doi:https://doi.org/10.1002/tcr.201600067.

29. Seah, J.W.K.; Teo, R.H.X.; Leung, P.-H. Organometallic chemistry and application of palladacycles in asymmetric hydrophosphination reactions. *Dalton Trans.* **2021**, doi:10.1039/D1DT03134A.

30. Pullarkat, S.A. Recent Progress in Palladium-Catalyzed Asymmetric Hydrophos-phination. *Synth.* **2016**, *48*, 493-503.

31. Bange, C.A.; Conger, M.A.; Novas, B.T.; Young, E.R.; Liptak, M.D.; Waterman, R. Light-Driven, Zirconium-Catalyzed Hydrophosphination with Primary Phosphines. *ACS Catal.* **2018**, *8*, 6230-6238, doi:10.1021/acscatal.8b01002.

32. Novas, B.T.; Bange, C.A.; Waterman, R. Photocatalytic Hydrophosphination of Alkenes and Alkynes Using Diphenylphosphine and Triamidoamine-Supported Zirconium. *Eur. J. Inorg. Chem.* **2019**, *2019*, 1640-1643, doi:10.1002/ejic.201801079.

33. Cibuzar, M.P.; Novas, B.T.; Waterman, R. Zirconium Complexes. In *Comprehensive Coordination Chemistry III*, Constable, E.C., Parkin, G., Que Jr, L., Eds.; Elsevier: Oxford, 2021; pp. 162-196.

34. Bange, C.A.; Waterman, R. Zirconium-catalyzed hydroarsination with primary arsines. *Polyhedron* **2018**, *156*, 31-34, doi:https://doi.org/10.1016/j.poly.2018.09.007.

35. Cibuzar, M.P.; Dannenberg, S.G.; Waterman, R. A Commercially Available Ruthenium Compound for Catalytic Hydrophosphination. *Isr. J. Chem.* **2020**, *60*, 446-451, doi:https://doi.org/10.1002/ijch.201900070.

36. Ackley, B.J.; Pagano, J.K.; Waterman, R. Visible-light and thermal driven double hydrophosphination of terminal alkynes using a commercially available iron compound. *Chem. Commun. (Camb)* **2018**, *54*, 2774-2776, doi:10.1039/c8cc00847g.

37. Zhang, Y.; Qu, L.; Wang, Y.; Yuan, D.; Yao, Y.; Shen, Q. Neutral and Cationic Zirconium Complexes Bearing Multidentate Aminophenolato Ligands for Hydrophosphination Reactions of Alkenes and Heterocumulenes. *Inorg. Chem.* **2018**, *57*, 139-149, doi:10.1021/acs.inorgchem.7b02248.

38. Zhang, Y.; Wang, X.; Wang, Y.; Yuan, D.; Yao, Y. Hydrophosphination of alkenes and alkynes with primary phosphines catalyzed by zirconium complexes bearing aminophenolato ligands. *Dalton Trans.* **2018**, *47*, 9090-9095, doi:10.1039/C8DT02122H.

39. Zhang, Y.; Sun, Q.; Wang, Y.; Yuan, D.; Yao, Y.; Shen, Q. Intramolecular hydroamination reactions catalyzed by zirconium complexes bearing bridged bis(phenolato) ligands. *RSC Adv.* **2016**, *6*, 10541-10548, doi:10.1039/C5RA23270H.

40. Waterman, R. Selective Dehydrocoupling of Phosphines by Triamidoamine Zirconium Catalyst. *Organometallics* **2007**, *26*, 2492-2494, doi:10.1021/om070189o.

354
355
356
357
358
359
360
361